Supplementary Information

Superlattice deformation in quantum dot films on flexible substrates via uniaxial strain

Julian E. Heger[a], Wei Chen[ab], Huaying Zhong[a], Tianxiao Xiao[a], Constantin Harder[ac], Fabian A. C. Apfelbeck[a], Alexander F. Weinzierl[a], Regine Boldt[d], Lucas Schraa[d], Eric Euchler[d], Anna K. Sambale[d], Konrad Schneider[d], Matthias Schwartzkopf[c], Stephan V. Roth[ce] and P. Müller-Buschbaum*[af]

[a.] Technical University of Munich, TUM School of Natural Sciences, Department of Physics, Chair for Functional Materials, James-Franck-Str. 1, 85748 Garching, Germany.

[b.] College of Engineering Physics, Shenzhen Technology University (SZTU), Lantian Road 3002, Pingshan 518118 Shenzhen, China

[c.] Deutsches Elektronen-Synchrotron DESY, Notkestraße 85, 22607 Hamburg, Germany

[d.] Leibniz-Institut für Polymerforschung Dresden e.V., Institut für Polymerwerkstoffe, Hohe Straße 6, 01069 Dresden, Germany

[e.] Royal Institute of Technology KTH, Teknikringen 34-35, 100 44 Stockholm, Sweden

[f.] Technical University of Munich, Heinz Maier-Leibnitz Zentrum (MLZ), Lichtenbergstraße 1, 85748 Garching, Germany
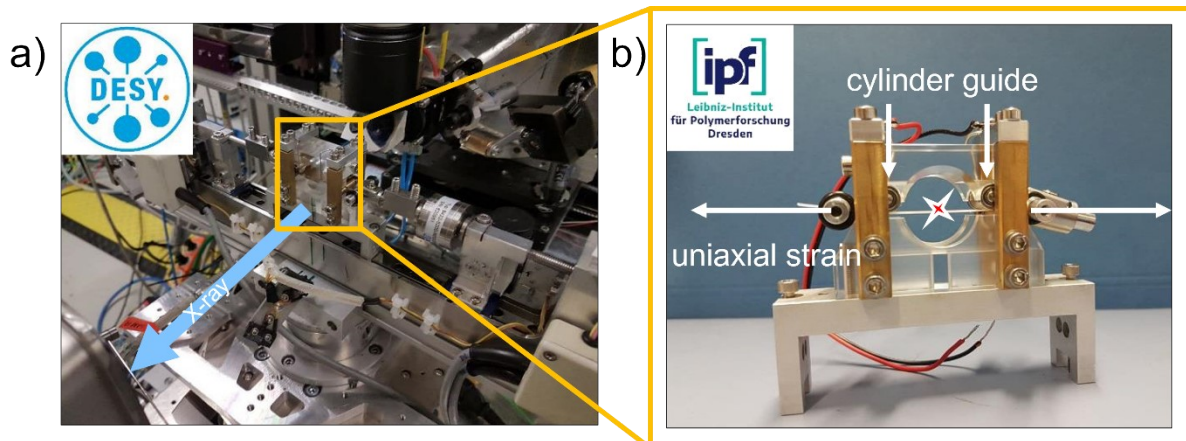
Fig. S1. Photographs of the experimental *in situ* GISAXS setup. a) Stretching apparatus based on two stepping motors for uniaxial stretching of the sample perpendicular to the incoming X-rays mounted at beamline P03. b) Sample holder designed for *in situ* GISAXS on freestanding, flexible substrates. Two pairs of cylindrical roles guide the sample during stretching and maintain sample alignment with respect to the X-ray beam. The sample is attached with clamps and fixed to the stepping motors for uniaxial stretching. A red star indicates the X-ray beam position on the thin quantum dot (QD) film.
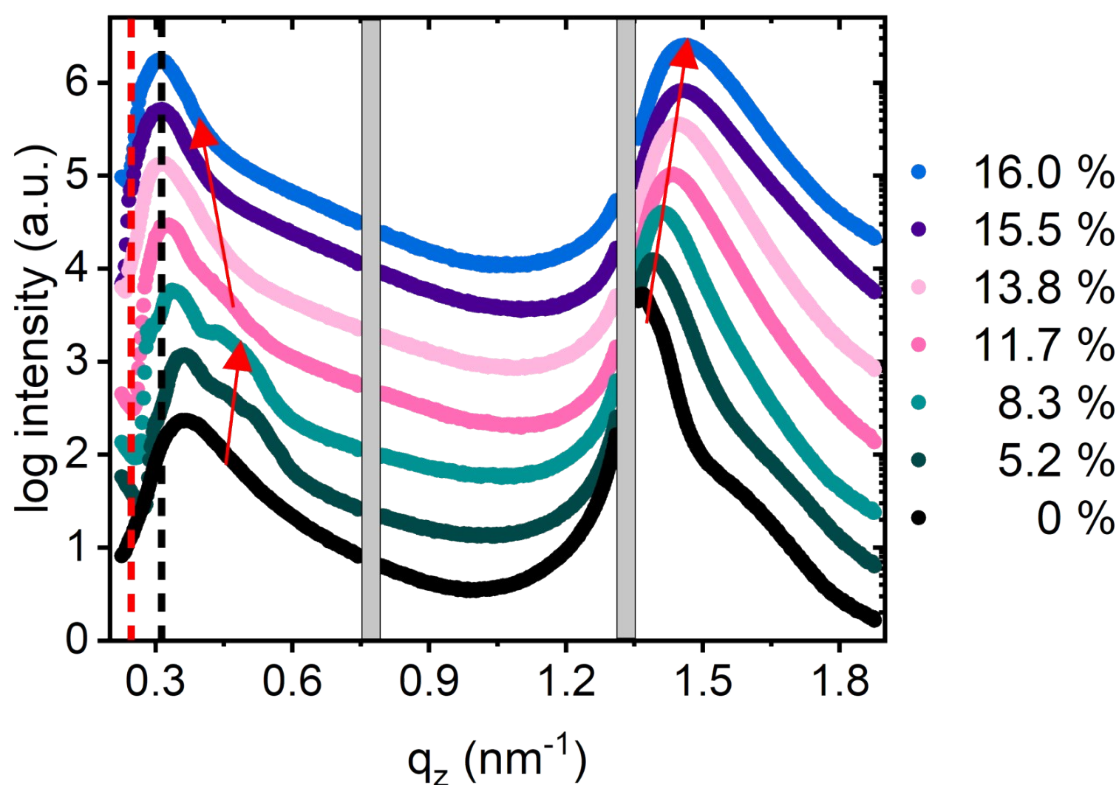
Fig. S2. Vertical GISAXS intensity with increasing effective strain. Vertical line cuts at $q_y = 0$ nm^{-1} are shown for the respective strain. The grey boxes mask the detector gaps. The red dashed line indicates the sample horizon. The Yoneda intensity at $q_z = 0.37$ nm^{-1} measures the sample's electron density. With increasing effective strain from 0 % to 8.3 %, an additional intensity at higher q_z values of about 0.45 nm^{-1} appears, as shown with a red arrow. This trend further confirms the increasing unit cell density along with the phase transition. The Yoneda intensities shifts towards lower q_z values from 11.7 % to 15.5 % of applied effective strain and remains constant at the black dashed line at 0.31 nm^{-1} afterward. The decreasing electron density after the phase transition reflects the increasing formation of voids with the beginning of crack propagation. The peak at $q_z = 1.4$ nm^{-1} shifting towards higher q_z corresponds to the (111) and (011) superlattice planes of the FCC and BCT unit cells, respectively.
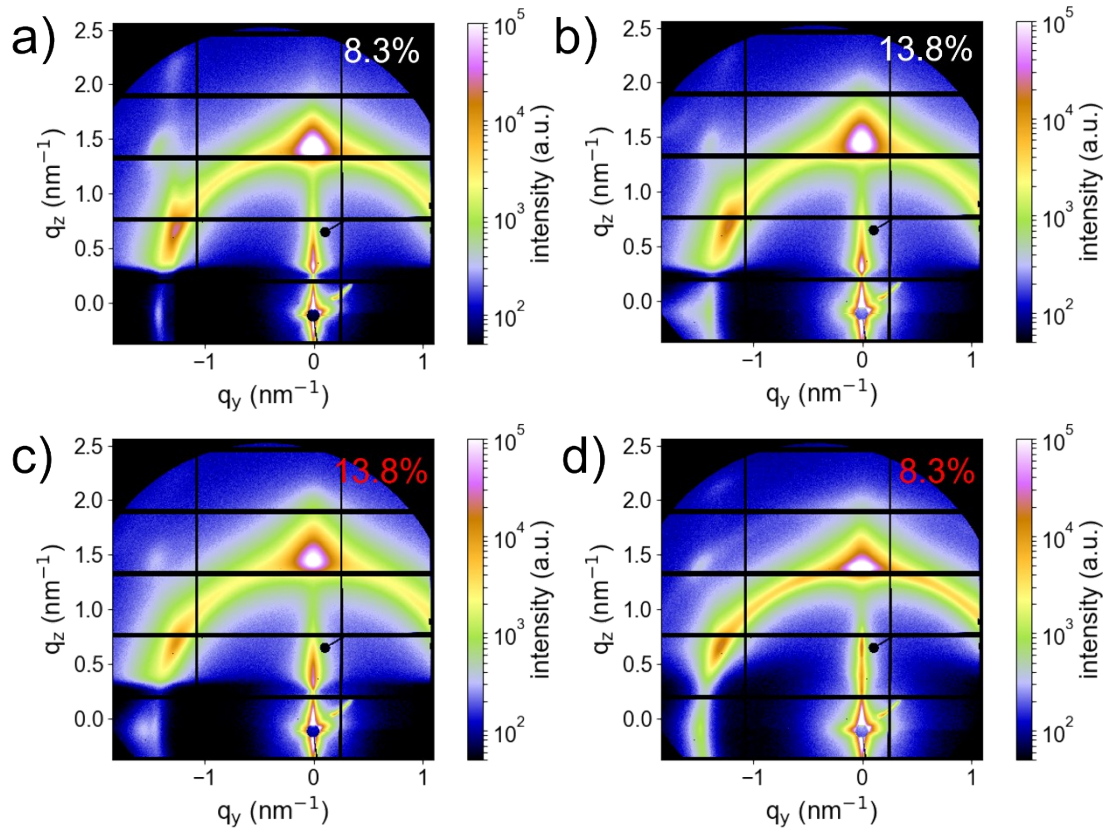
Fig. S3. Relaxed superlattice deformation. The superlattice deformation passing the FCC/BCT-BCC-BCT phase transition from a) 10 % of substrate elongation with the effective strain of 8.3 % to b) 20 % (the effective strain of 13.8 %), discussed in the main text, shows a relaxation of superlattice deformation in the 2D GISAXS data when releasing the substrate elongation from c) 20 % back to d) 10 %.
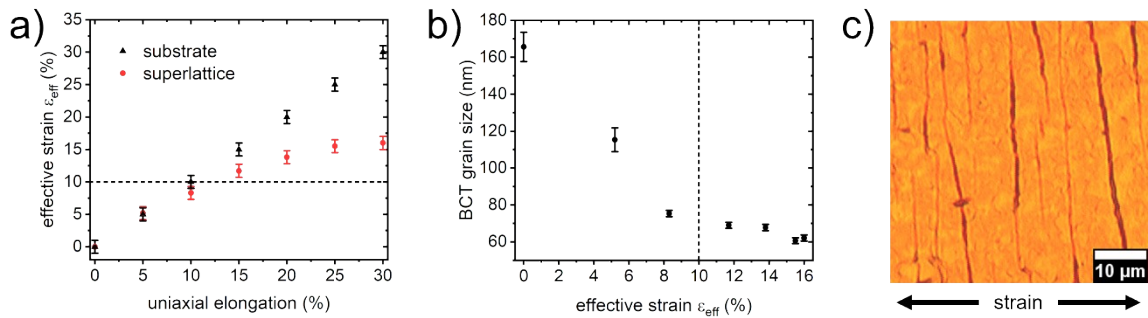
Fig. S4. Effective strain applied to the superlattice. a) Comparison of the effective strain applied to the superlattice and to the substrate show increasing deviation starting from 10 % of substrate elongation. The applied strain increasingly distributes on crack formation on which it is fully focused at 30 %. The maximum effective strain applied to the superlattice is 16 %. b) Besides the average superlattice domains, which are formed by the QDs around the average size of 2.7 nm, domains of larger PbS QDs pass the phase transition locally already at lower applied strain. This effect leads to peak broadening of the lattice reflexes in GISAXS and contributes to the early formation of grain boundaries towards 10 %. Average grain size obtained from Scherrer analysis. With the reduction in grain size to 10 %, grain boundaries are formed. Since only a few grain boundaries are formed after 10 %, they play a minor role in strain distribution at higher strains. c) Optical microscopy image of the PbS QD film after stretching reveals elongated cracks that are orthogonal to the direction of applied strain in a distance of 5 to 10 µm.
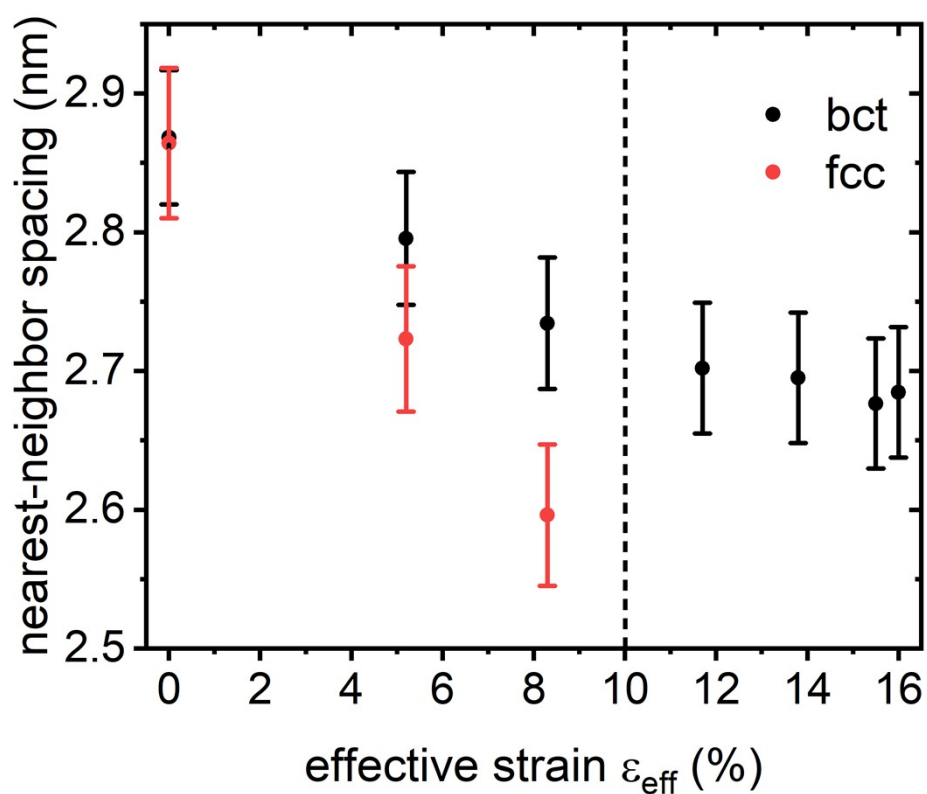
Fig. S5. Nearest-neighbor spacing with increasing effective strain. The edge-to-edge distance of nearest-neighbor QDs is the same for BCT and FCC in the nested unit cell configuration at 0 %. With increasing superlattice deformation, BCT and FCC nearest neighbors separate. Both spacings indicate a high degree of intercalation and compression of the ligands having a relaxed chain length of 2.5 nm. The compression level finally reaches a critical value for the FCC phase, which triggers the phase transition at 10 %.
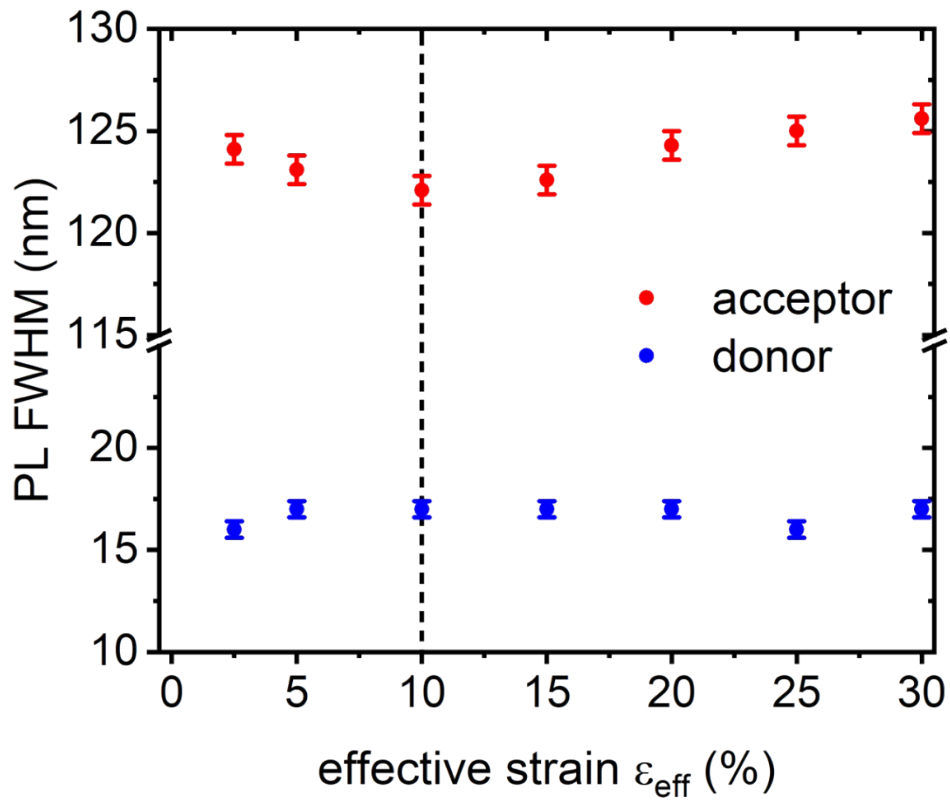
Fig. S6. *In situ* PL emission broadening with effective strain. A slight decrease of PL FWHM is found for the acceptor until 10 %, followed by an increase afterwards, whereas it remains constant for the donor. With increased unit cell isotropy, donor-acceptor couples can form more uniformly with respect to their size difference. With increasing crack propagation, more donor-acceptor couples at crack interfaces rearrange, leading to an increased broadening of the acceptor emission.
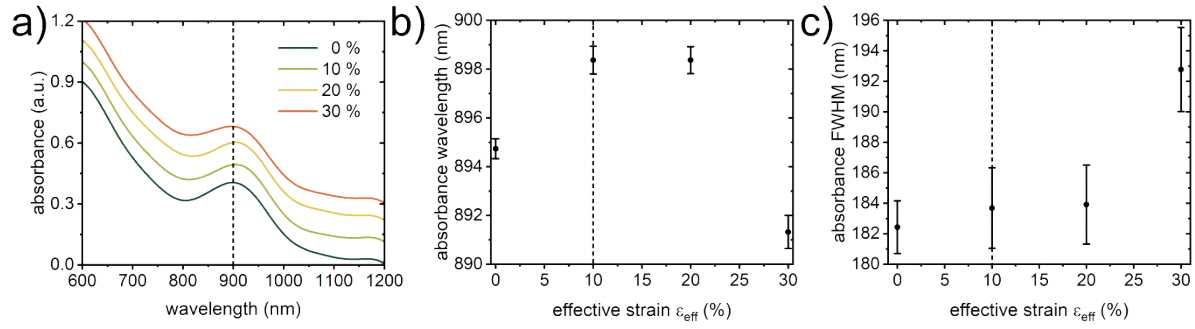
Fig. S7. *In situ* absorbance spectra with increasing strain. a) First excitonic peak in the absorbance spectra of PbS QD films shows a slight shift with the increasing effective strain. The curves are fitted with Gaussian functions to extract the evolution of center wavelengths and the corresponding FWHM. b) The absorbance wavelength redshifts towards the phase transition at 10 % by about 4 nm, remains constant at 20 %, and blueshifts by about 6 nm at 30 %. The occurring redshift corresponding to about 6 meV and its correlation with the decreasing edge-to-edge distance of nearest neighbors (Figure S5) is in good agreement with the observed redshift via decreasing inter-dot distance upon ligand exchange in PbSe QD thin films.[1] c) The FWHM remains constant within the error bars and broadens at 30%. We attribute the blueshift and line broadening at 30 % to the increasingly contributing interfaces at the microscopic cracks.
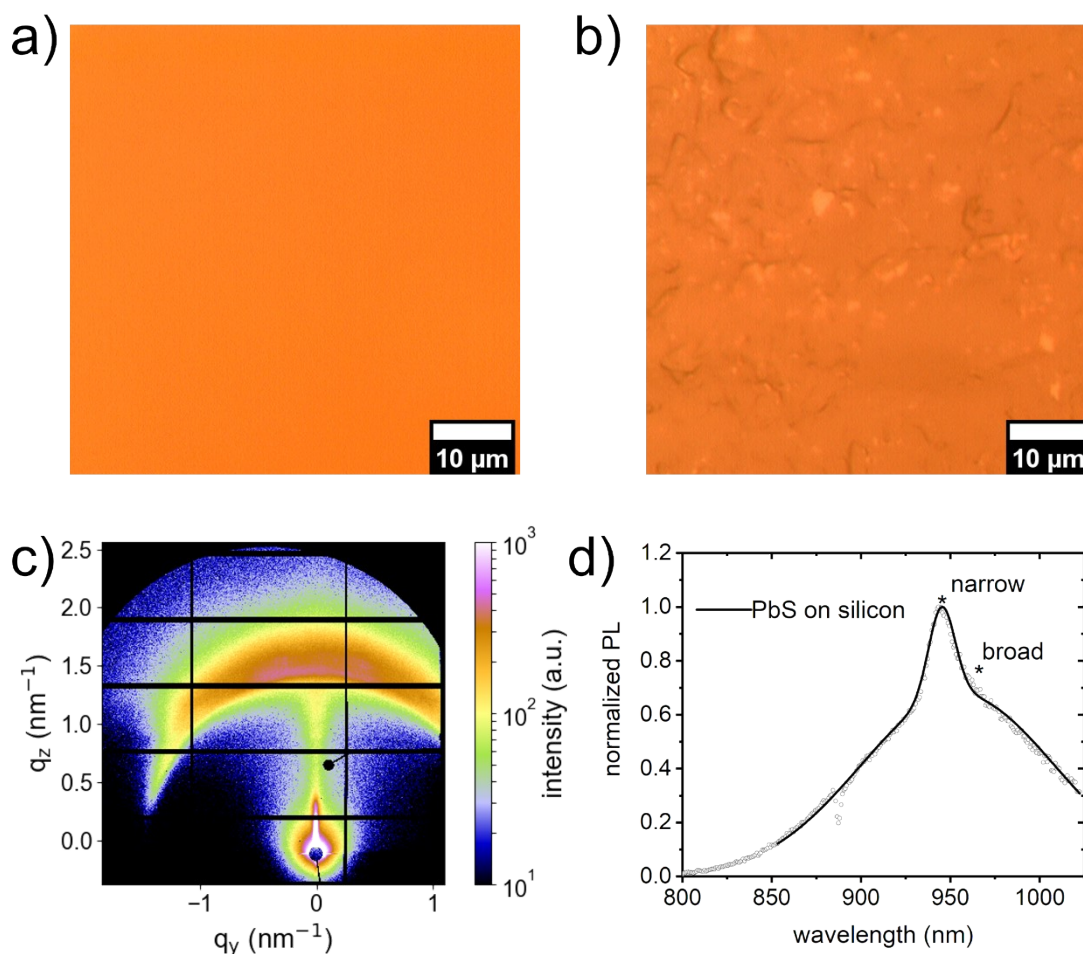
Fig. S8. Influence of the substrate on superlattice and PL. a) Optical microscopy image of a custom-made PDMS substrate, as used for the *in situ* GISAXS, *in situ* PL, and *in situ* absorbance measurements, shows the smooth and homogeneous surface necessary to form the superlattices investigated. b) Optical microscopy image of a commercially available PDMS substrate used as a reference. The heterogeneous surface does not provide superlattices with defined unit cells and long-range order. c) 2D GISAXS data of PbS QDs spin-coated on the commercial PDMS reference substrate. The scattering intensity shows a single reflex with strong azimuthal and radial broadening, indicating weak long-range order and poor superlattice formation. Moreover, the substrate's surface chemistry also influences the PbS QD film's adhesion and hence influences grain boundary formation during spin-coating and stretching. While grain boundaries play a minor role in the observed strain distribution, the biggest effect of the substrate is on the observed superlattice deformation in the actual superlattice formation beforehand. d) Reference PL spectrum of PbS QDs spin-coated on a silicon substrate shows good agreement with the *in situ* PL spectrum on custom-made PDMS.
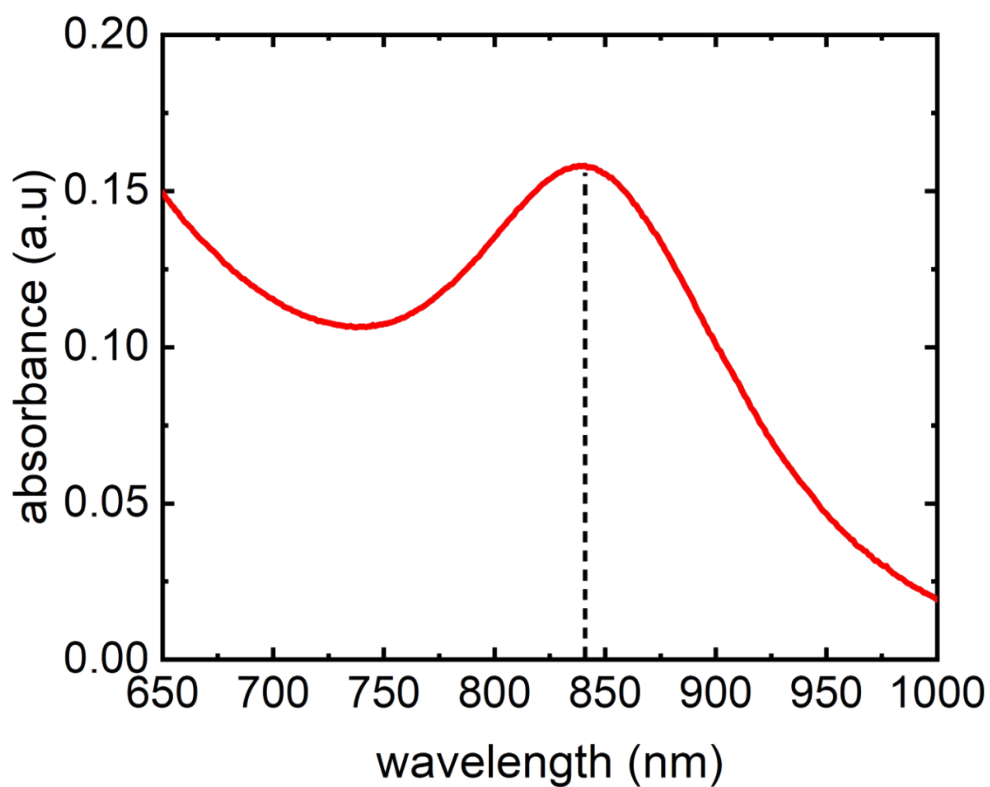
Fig. S9. PbS QDs absorbance spectrum. The absorbance spectrum was taken from solid films from the same batch used for *in situ* GISAXS and *in situ* PL experiments. We used the Weidman model to calculate the size from the absorption spectra.[2] The average QD size of (2.70 ± 0.02) nm is obtained from the absorbance center and agrees with the TEM results obtained from another batch of PbS that was prepared according to the same protocol.

Superlattice index matching on 2D GISAXS data with GIXSGUI

We use the MATLAB software GIXSGUI for indexing the observed superlattice reflexes on the 2D GISAXS data.[3] GIXSGUI is a broadly used application for treating raw data from grazing incidence scattering. It offers a variety of functions, such as transferring the data from as-measured pixel space to reciprocal q-space, plotting the data in various representations, and indexing the reflexes in a scattering pattern. The graphical user interface of GIXSGUI is opened with the function *gixsgui* in MATLAB Command Window, after loading the path to GIXSGUI with subfolders to the MATLAB editor (**Fig. S10**). For more information about the installation of GIXSGUI and the available functions, we recommended the software documentation:

https://www.aps.anl.gov/files/APS-Uploads/SECTOR8/8-ID/doc.pdf

In the following, we present a step-by-step guide about how we use GIXSGUI to identify the superlattice unit cells, which are discussed in this work. The routine is summed up in three main steps: 1. Enter the setup parameters for scattering geometry and detector details. 2. Calculate the superlattice reflexes for a given space group in q-space. 3. Plot selected superlattice indices on the 2D GISAXS data in q-space representation.

1. Enter the setup parameters for scattering geometry and detector details (**Fig. S11**).

1.1. The setup parameters must be entered in the top right corner of the appearing window. These parameters include the sample-detector distance, X-ray energy, incident angle, direct and specular beam positions, and detector details about, e.g., pixel size. This information is obtained by calibration measurements at the DESY P03 beamline and from the Pilatus 2M detector datasheet.

1.2. For convenience, the setup parameters are saved and exported so that they are easy to reload next time. The working directory is loaded via the path to the 2D GISAXS data. In this step-by-step guide, we exemplarily use the GISAXS data at 0 %, 10 %, and 30 % of applied strain to the substrate.

1.3. The 2D GISAXS data is loaded and plotted in q-space representation on a logarithmic intensity scale by choosing the respective plot settings and double click on the respective data file.

2. Calculate the superlattice reflexes for a given space group in q-space (**Fig. S12-S15**).

2.1. By clicking on the Data Processing button, an additional window appears, in which the Diffraction tab is selected for calculating the superlattice reflexes.

2.2. The parameters for the unit cell's space group and superlattice constant are entered. This is an iterative process, which starts with an educated guess based on our previous work and becomes defined with the superlattice constants, which are obtained from the measured q-positions of the reflexes.[4] The q-positions are obtained by Gaussian fits of the reflexes 1D peak intensities, which are in this work azimuthally integrated by using the software DPDAK.[5] We choose the space group #139 (I 4/mmm) with $a = b \neq c$ describing a distorted BCC unit cell to match the shifting reflexes of the BCT-BCC-BCT phase transition with increasing strain (Fig. S12, S13, S14). To match the remaining scattering pattern in the nested FCC/BCC symmetry before the phase transition, we use space group #225 (Fm-3m) with $a = b = c$, describing the FCC unit cell (Fig. S15).

2.3. It is necessary to enter the unit cell orientation with respect to the substrate. In this work, the (011) planes of the distorted BCC unit cell and the (111) planes of the FCC unit cell are parallel to the substrate in edge-on and corner-on orientation, respectively. After setting the set of indices to be calculated, the calculation can be started with the respective button Start Calculation.

3. Plot selected superlattice indices on the 2D GISAXS data in *q*-space representation (Fig. S12-S15).

3.1. The calculated set of indices can be plotted on the 2D GISAXS data in *q*-space representation when choosing the plot option Born. Spare indices of the calculated set, which are not present in the 2D GISAXS data, are deselected from the table.

3.2. Further adjustments of the intensity scale and its color code can be made in the appearing window of the combined 2D GISAXS and superlattice indices plot. When the indices match the reflex positions, the process of index matching with GIXSGUI is done.
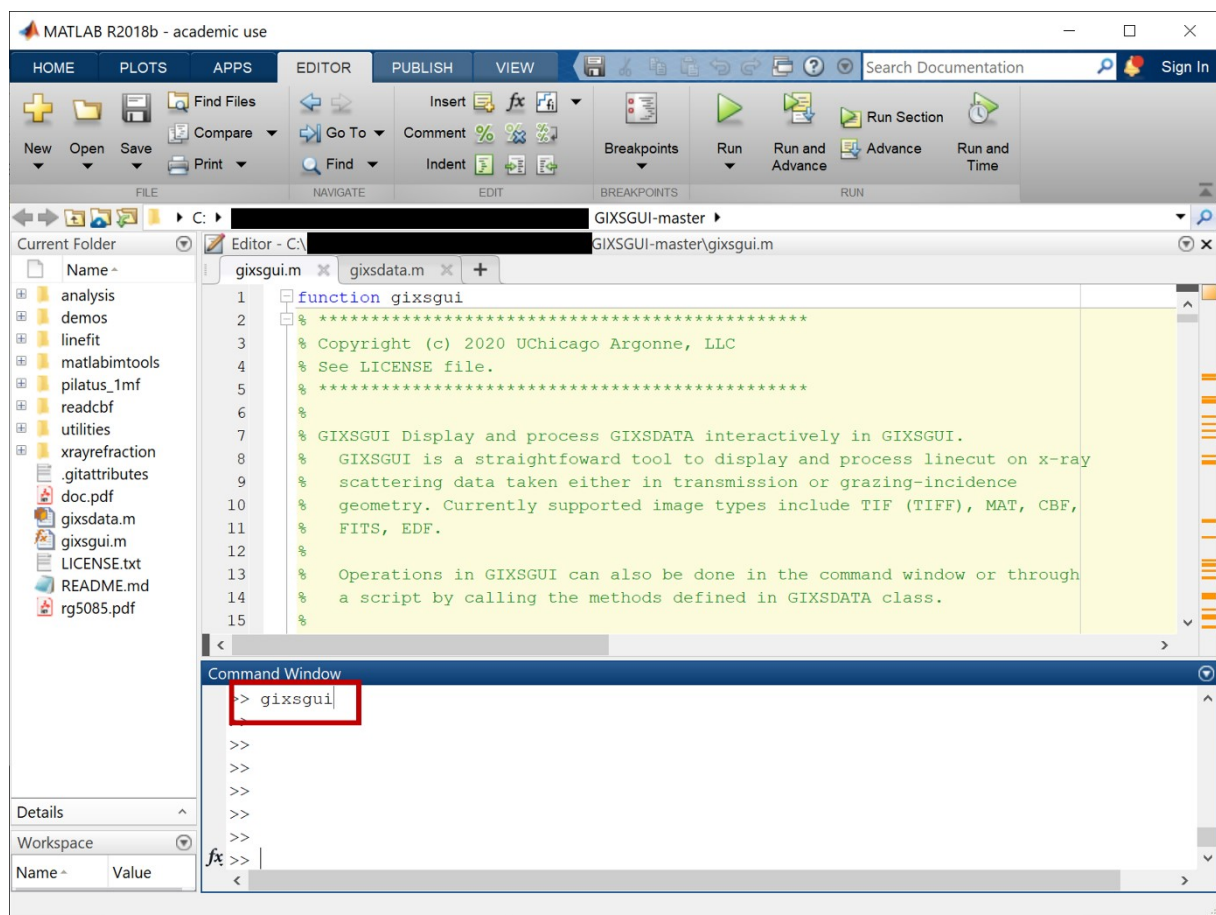
Fig. S10. GIXSGUI is started by loading its path with subfolders to the editor environment of MATLAB. The function *gixsgui* highlighted by the red box opens the graphical user interface.
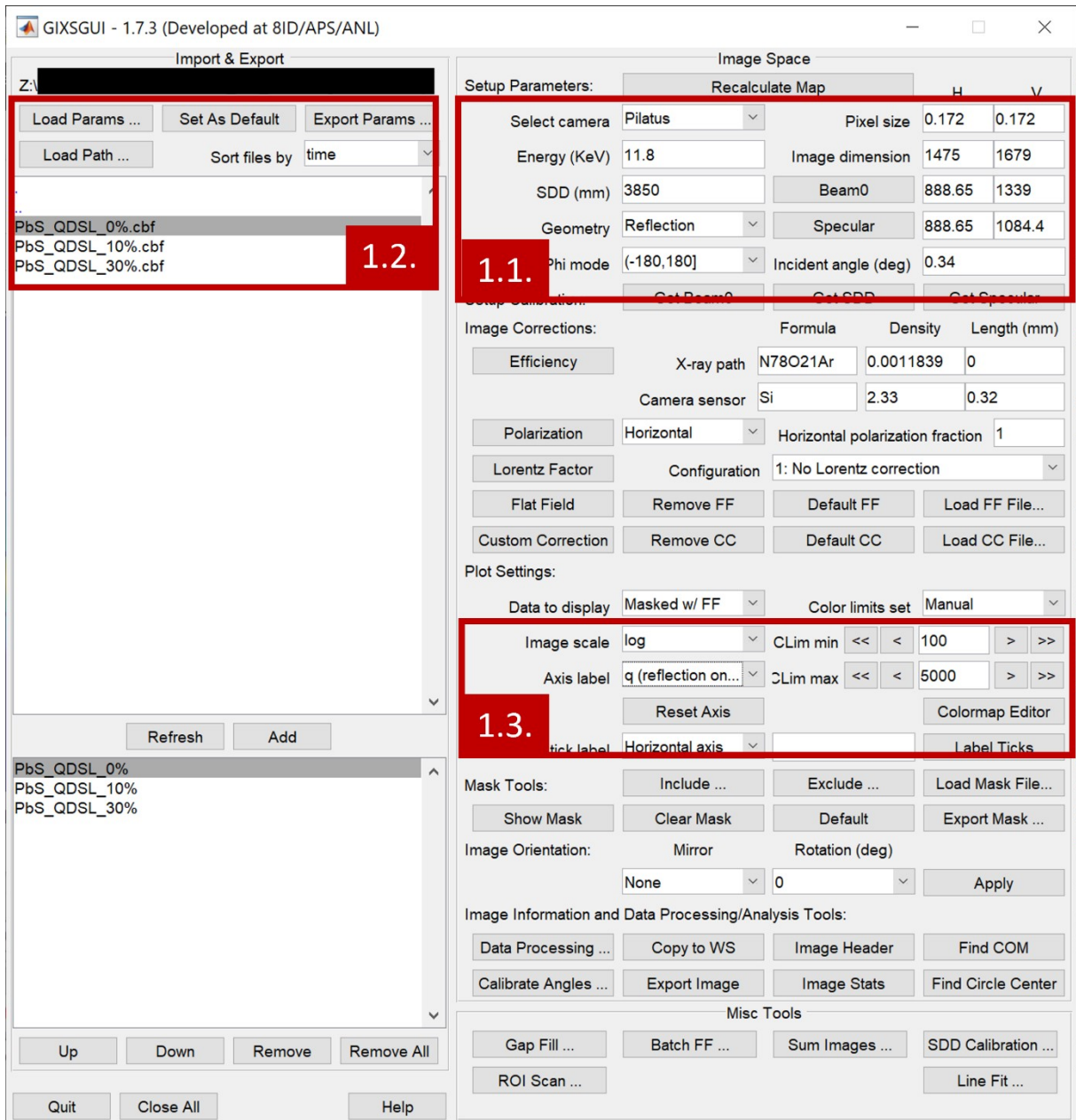
Fig. S11. The setup parameters are entered, and the working directory is opened in the main window. The 2D GISAXS data is loaded and plotted from the working directory. The button Data Processing opens a window where index calculation is done. The numbers label the steps as explained in the step-by-step guide.
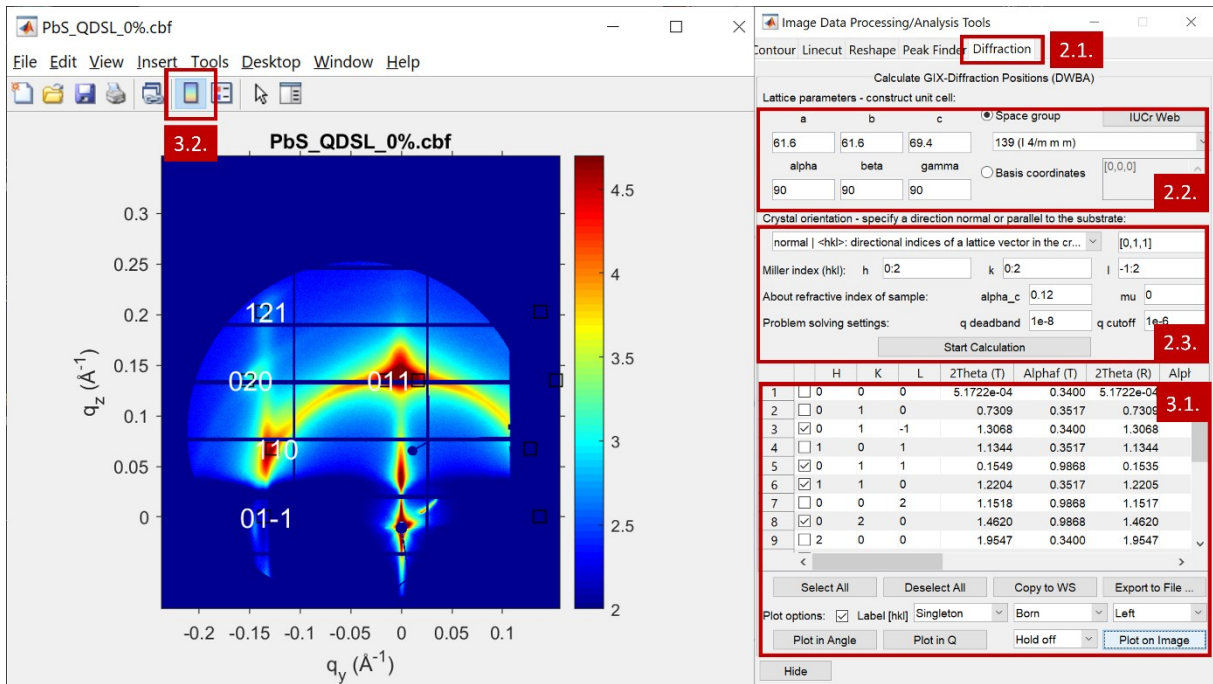
Fig. S12. The superlattice indices for the (121), (020), (110), (011), and (00-1) planes for the distorted BCC unit cell in space group #135 with edge-on orientation are matched with GIXSGUI and plotted on the 2D GISAXS data without applied strain. The superlattice constants a = b = 61.6 Å , and c = 69.4 Å are obtained from the center values of the q_{011} and q_{110} reflexes. The numbers label the steps as explained in the step-by-step guide.
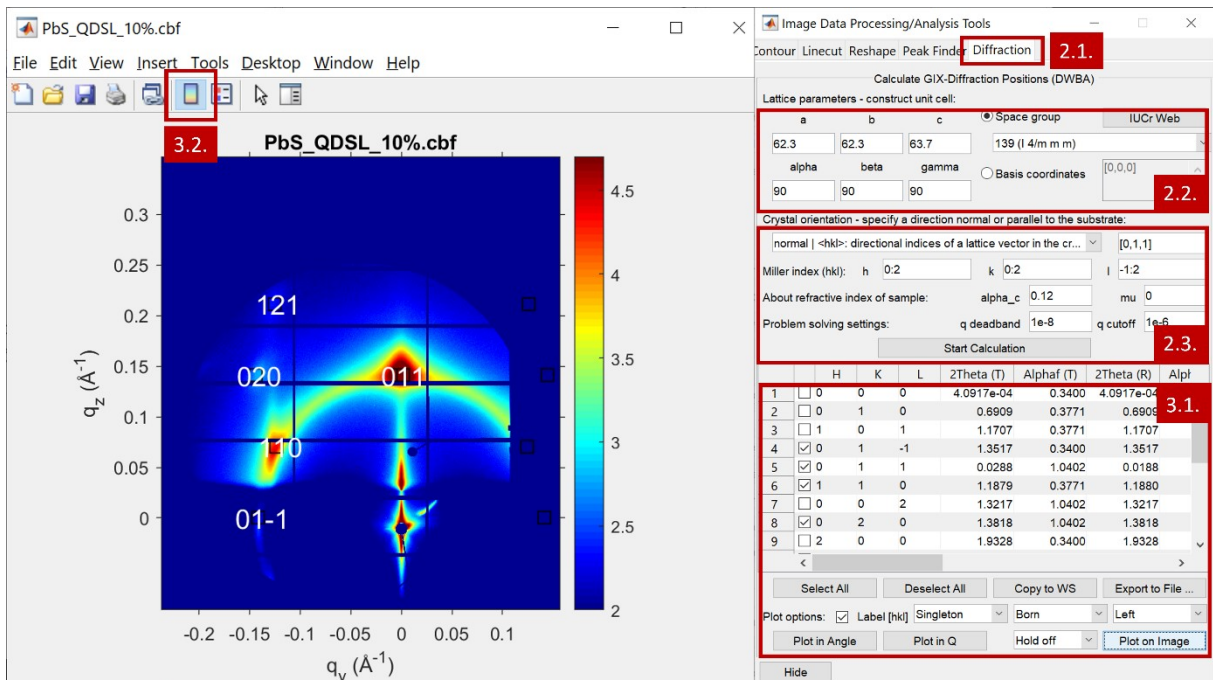
Fig. S13. The superlattice indices for the (121), (020), (110), (011), and (00-1) planes for the distorted BCC unit cell in space group #135 with edge-on orientation are matched with GIXSGUI and plotted on the 2D GISAXS data at 10 % applied strain, close to the BCT-BCC-BCT phase transition. The superlattice constants a = b = 62.3 Å , and c = 63.7 Å are obtained from the center values of the q_{011} and q_{110} reflexes. The numbers label the steps as explained in the step-by-step guide.
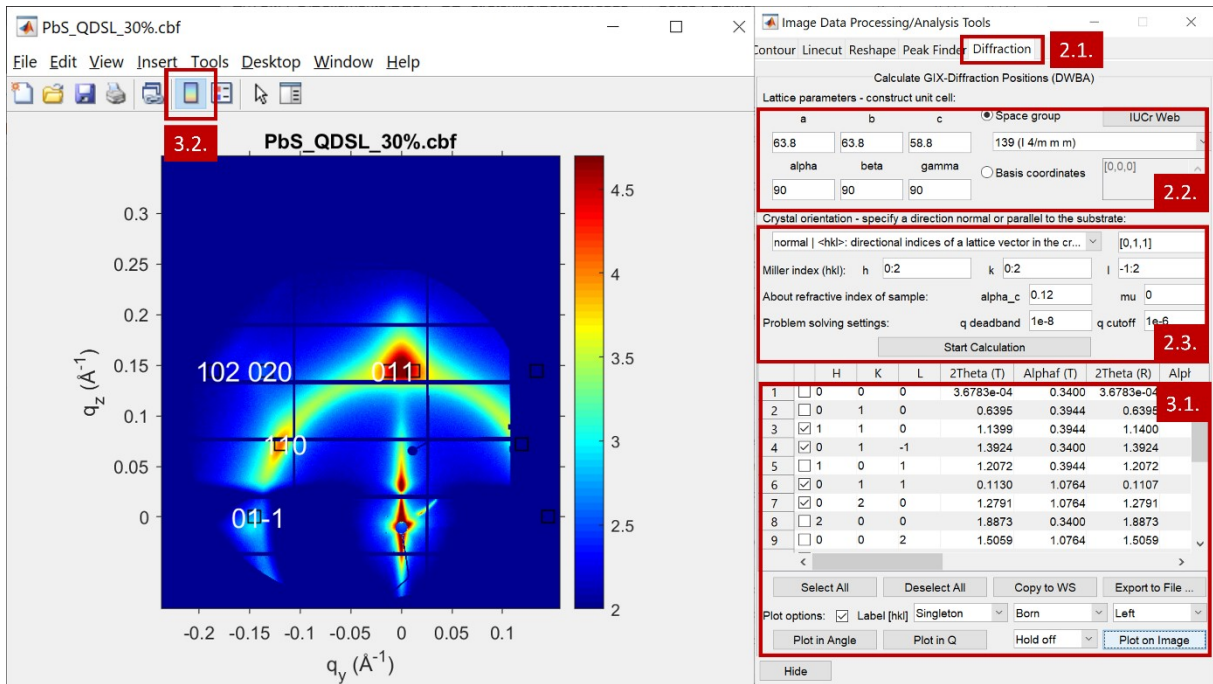
Fig. S14. The superlattice indices for the (121), (020), (110), (011), and (00-1) planes for the distorted BCC unit cell in space group #135 with edge-on orientation are matched with GIXSGUI and plotted on the 2D GISAXS data at maximum applied strain. The superlattice constants a = b = 63.8 Å , and c = 58.8 Å are obtained from the center values of the q_{011} and q_{110} reflexes. The numbers label the steps as explained in the step-by-step guide.
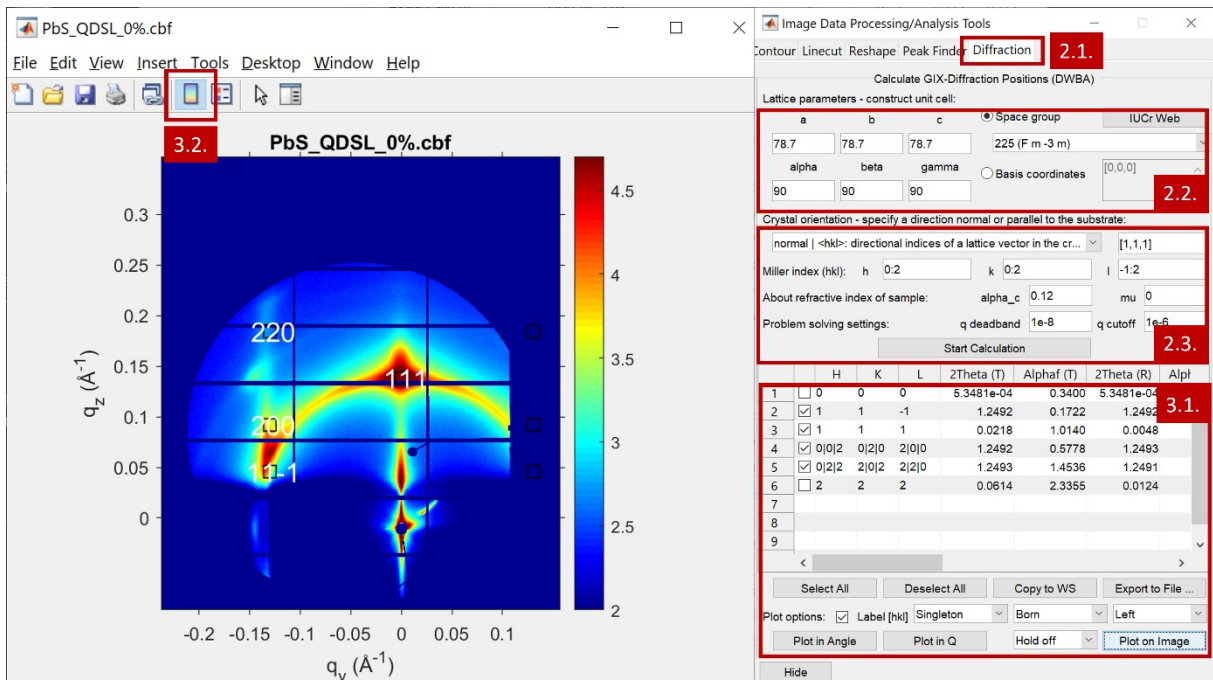
Fig. S15. The superlattice indices for the (220), (200), (11-1), and (111) planes for the FCC unit cell in space group #225 with corner-on orientation are matched with GIXSGUI and plotted on the 2D GISAXS data without applied strain. The superlattice constants a = b = c = 78.7 Å are obtained from the center values of the q_{111} reflex. The numbers label the steps as explained in the step-by-step guide.

References:

1   A. Wolcott, V. Doyeux, C. A. Nelson, R. Gearba, K. Wai Lei, K. G. Yager, A. D. Dolocan, K. Williams, D. Nguyen and X.-Y. Zhu, *J. Phys. Chem. Lett.*, 2011, **2**, 795-800.

2   M. C. Weidman, M. E. Beck, R. S. Hoffman, F. Prins, W. A. Tisdale, Monodisperse, *ACS Nano*, 2014, **8**, 6363-6371

3   Z. Jiang, *J. Appl. Cryst.*, 2015, **48**, 917–926

4   W. Chen, H. Tang, Y. Chen, J. E. Heger, N. Li, L. P. Kreuzer, Y. Xie, D. Li, C. Anthony, Z. Pikramenou, K. W. Ng, X. W. Sun, K. Wang and P. Müller-Buschbaum, *Nano Energy*, 2020, **78**, 105254.

5.   G. Benecke, W. Wagermaier, C. Li, M. Schwartzkopf, G. Flucke, R. Hoerth, I. Zizak, M. Burghammer, E. Metwalli, P. Müller-Buschbaum, M. Trebbin, S. Förster, O. Paris, S. V. Roth and P. Fratzl, *J. Appl. Cryst.*, 2014, **47**, 1797–1803.